UC Davis
UC Davis Previously Published Works

Title

Cellular transformation promotes the incorporation of docosahexaenoic acid into the endolysosome-specific lipid bis(monoacylglycerol)phosphate in breast cancer

Permalink

https://escholarship.org/uc/item/9wr544pf

Authors

Berg, Anastasia L
Showalter, Megan R
Kosaisawe, Nont
et al.

Publication Date

2023-03-01

DOI

10.1016/j.canlet.2023.216090

Peer reviewed

eScholarship.org Powered by the California Digital Library
University of California

Author Manuscript
Author Manuscript
Author Manuscript
Author Manuscript

HHS Public Access
Author manuscript
Cancer Lett. Author manuscript; available in PMC 2024 March 31.

Published in final edited form as:
Cancer Lett. 2023 March 31; 557: 216090. doi:10.1016/j.canlet.2023.216090.

Cellular transformation promotes the incorporation of docosahexaenoic acid into the endolysosome-specific lipid bis(monoacylglycerol)phosphate in breast cancer

Anastasia L. Berg[1,*], **Megan R. Showalter**[2,*], **Nont Kosaisawe**[3], **Michelle Hu**[1], **Nathanial C. Stephens**[2], **Michael Sa**[2], **Hailey Heil**[2], **Noemi Castro**[1], **Jenny J. Chen**[1], **Kacey VanderVorst**[1], **Madelyn R. Wheeler**[1], **Zachary Rabow**[2], **Tomas Cajka**[2,4], **John Albeck**[3], **Oliver Fiehn**[2], **Kermit L. Carraway III**[1,#]

[1]Department of Biochemistry and Molecular Medicine, and UC Davis Comprehensive Cancer Center, University of California Davis School of Medicine, Sacramento, CA, USA

[2]West Coast Metabolomics Center, UC Davis Genome Center, University of California Davis, Davis, CA, USA

[3]Department of Molecular and Cellular Biology, University of California Davis, Davis, CA, USA

[4]Current address: Institute of Physiology of the Czech Academy of Sciences, Prague, 14200, Czech Republic

Abstract

Bis(monoacylglycero)phosphates (BMPs), a class of lipids highly enriched within endolysosomal organelles, are key components of the lysosomal intraluminal vesicles responsible for activating sphingolipid catabolic enzymes. While BMPs are understudied relative to other phospholipids, recent reports associate BMP dysregulation with a variety of pathological states including neurodegenerative diseases and lysosomal storage disorders. Since the dramatic lysosomal remodeling characteristic of cellular transformation could impact BMP abundance and function, we employed untargeted lipidomics approaches to identify and quantify BMP species in several *in vitro* and *in vivo* models of breast cancer and comparative non-transformed cells and tissues. We observed lower BMP levels within transformed cells relative to normal cells, and consistent enrichment of docosahexaenoic acid (22:6) fatty acyl chain-containing BMP species in both human- and mouse-derived mammary tumorigenesis models. Our functional analysis points to a working model whereby 22:6 BMPs serve as reactive oxygen species scavengers in tumor cells, protecting lysosomes from oxidant-induced lysosomal membrane permeabilization. Our findings suggest that breast tumor cells might divert polyunsaturated fatty acids into BMP lipids as part of an adaptive response to protect their lysosomes from elevated reactive oxygen species levels, and raise the possibility that BMP-mediated lysosomal protection is a tumor-specific vulnerability that may be exploited therapeutically.

[#]To whom correspondence should be addressed: Dr. Kermit Carraway, Department of Biochemistry and Molecular Medicine, UC Davis School of Medicine, Sacramento, CA 95817 USA, Ph: 1-916-734-3114, klcarraway@ucdavis.edu.
[*]These authors contributed equally.

Competing interests
The authors declare no competing financial interests.

Author Manuscript Author Manuscript Author Manuscript Author Manuscript

Keywords

breast cancer; bis(monoacylglycerol)phosphate; BMP; lipidomics; lysosomal membrane permeabilization; polyunsaturated fatty acids; reactive oxygen species

Introduction

Bis(monoacylglycero)phosphate (BMP; originally named lysobisphosphatidic acid, LBPA), considered a structural isomer of phosphatidylglycerol, was originally discovered over fifty years ago[1] but has remained understudied compared to more prevalent regulatory phospholipids such as ceramides and phosphatidylinositols. However, emerging evidence suggests that BMP class phospholipids perform critical roles in mammalian lysosomal function and stability, and are modulated in several disease states[2,3]. BMPs comprise a minor component (approximately 1–2%) of total cellular membrane lipids but are highly enriched in late endosomes and lysosomes where they comprise up to 15% of lipid content[4]. While BMP metabolism remains largely undefined, it has been reported that BMPs are synthesized in late endosomes from phosphatidylglycerol (PG)[5] and metabolized by the lipase ABHD6 with the release of free fatty acids[6]. BMPs play a key structural role in the formation of the intraluminal vesicles (comprising 70% of total vesicular lipid content) that accumulate within endo-lysosomal organelles, where they serve as docking site activators for luminal acid hydrolases involved in glycolipid breakdown[7,8].

BMPs are structurally diverse and consist of varied fatty acyl chain substituents. Interestingly, the fatty acyl composition of BMP appears to drive its precise biochemical function within cells[9,10]. BMPs predominantly contain oleic acid (fatty acid [FA] 18:1)[11–16], but BMP composition is dynamically regulated, with altered incorporation of the polyunsaturated fatty acids (PUFAs) linoleic acid (FA 18:2), arachidonic acid (FA 20:4), and docosahexaenoic acid (DHA; FA 22:6) observed in response to dietary changes[15], drug treatment[16,17], cellular stress[18], and various pathological conditions including lysosomal storage disorders (LSDs)[19]. BMPs have been investigated as markers of LSDs, as changes in both BMP acyl chain composition and total abundance are observed with disease onset in multiple LSD models[19,20]. Intriguingly, it has been reported that fatty acyl chain composition determines BMP stability under oxidative stress conditions, with PG-18:1/18:1 or PG-22:6/22:6 supplementation driving changes in BMP acyl chain composition and conferring varied sensitivity to oxidative stress-induced breakdown in macrophages[18].

The genesis and progression of tumors involves the significant expansion of the lysosomal compartment and alterations in lysosome quantity, composition, subcellular localization, lipid metabolism, and activity of luminal enzymes. These changes confer growth and survival advantages to the cancer cell, and have been demonstrated to promote tumor aggressiveness, angiogenesis, and metastasis[21,22]. In this regard, lysosomes harbor digestive enzymes that are critical for catabolism and recycling of intracellular and extracellular components, processes required for rapid tumor cell proliferation, invasiveness and nutrient consumption. On the other hand, high intracellular levels of reactive oxygen species (ROS) that induce the disruption of the limiting lysosomal membrane (lysosomal membrane

Author Manuscript Author Manuscript Author Manuscript Author Manuscript

permeabilization, LMP) and the release of luminal enzymes into the cytosol can trigger cell death through apoptotic and necrotic mechanisms[21,23,24].

As BMPs are vital to the maintenance of lysosome stability and function, and chronic cellular oxidative stress is a common feature of cancer and can potentially destabilize the lysosomal membrane, we set out to assess transformation-induced alterations in BMP content and diversity.

Materials & Methods

Cell culture and media

MDA-MB-231, MCF7, and SKBR3 cells were purchased from American Type Culture Collection (ATCC, Manassas, VA, USA) and maintained as recommended in 10% CO_2 in media supplemented with 10% fetal bovine serum (Genesee Scientific) and antibiotics (penicillin/streptomycin; Gibco, Thermo Fisher). MCF10A (ATCC) cells were maintained in mammary epithelial basal media (DMEM/F12; SH30023, HyClone) supplemented with 5% horse serum (16050–122, Invitrogen), 20ng/mL recombinant human epidermal growth factor (AF-100–15, PeproTech), 0.5 mg/mL hydrocortisone (H0999, Sigma Aldrich), 100ng/mL cholera toxin (C8052, Sigma Aldrich), and 10μg/mL insulin (I9278, Sigma Aldrich). Cell lines were authenticated prior to use by short-tandem repeat profiling (Genetics Core Facility; University of Arizona, Tucson, AZ, USA) and were replaced with a cryopreserved stock every six passages. Cell line attributes are summarized in Supplementary Table S1.

For live microscopy experiments, cells were maintained in a custom media formulation termed ‘imaging base-DMEM/F12’, which consists of DMEM/F12 lacking glucose, glutamine, riboflavin, folic acid, and phenol red (UC Davis Veterinary Medicine Biological Media Service) to eliminate background fluorescence. MCF10A cells were maintained in ‘imaging medium’ supplemented with 17mM glucose for all imaging experiments. Prior to microscopy analysis, cells were washed twice with their respective growth media, and then cultured in specialized imaging media for at least 2 hours prior to imaging, unless otherwise indicated. The cell to media ratio was maintained at 150–200 cells/μl for all experiments.

Immunofluorescence microscopy

Cells were grown to 70% confluence on glass coverslips, fixed for 20 minutes at room temperature in 4% paraformaldehyde, and blocked in 50mM ammonium chloride for 10 minutes and subsequently 0.1% bovine serum albumin in phosphate-buffered saline (PBS) for 20 minutes. Cells were incubated with primary antibodies anti-BMP/LBPA antibody clone 6C4 (MABT837, Millipore Sigma; 1/100), anti-LAMP1 (L1418, Sigma-Aldrich; 1:100) and anti-Rab7 D95F2 (9367, Cell Signaling; 1/100) in PBS containing 0.5% saponin for 30 minutes at room temperature. Following incubation with Alexa Fluor secondary antibodies (1:1000) for 30 minutes, cells were mounted in 4′,6-diamidino-2-phenylindole (DAPI) Fluoromount-G (0100–20, Southern Biotech). Samples were imaged with a Zeiss LSM 710 AxioObserver confocal microscope and analyzed with ZenBlue software.

Author Manuscript Author Manuscript Author Manuscript Author Manuscript

Live-cell fluorescence microscopy

Time-lapse wide-field microscopy was performed as described previously[25,26]. Briefly, 25,000 cells were plated 24 hours prior to imaging in glass-bottom 96-well plates (P96–1.5H-N, Cellvis, Mountain View, CA) pretreated with type I collagen (A10483–01, Gibco) to promote cell adherence. For analysis of lysosomal content, cells were incubated with 50nM LysoTracker Red DND-99 (L7528, Invitrogen) and 1μg/mL Hoechst 33342 (62249, Thermo Fisher) for nuclear counterstain. Cells were maintained in 95% air and 5% CO_2 at 37°C in an environmental chamber. Images were collected with a Nikon (Tokyo, Japan) 20/0.75 NA Plan Apo objective on a Nikon Eclipse Ti inverted microscope, equipped with a Lumencor SOLA or Lumencor SPECTRA X light engine. Fluorescence filters used in experiments were: DAPI (custom ET395/25x - ET460/50m - T425lpxr, Chroma), cyan fluorescence protein (CFP) (49001, Chroma), Sapphire (custom ET420/10x - ET525/50m - T425lpxr, Chroma), green fluorescence protein (GFP) (49002; Chroma), yellow fluorescence protein (YFP) (49003, Chroma), Cherry (41043, Chroma) and Cy5 (49006, Chroma). Images were acquired using Andor Zyla 5.5 scMOS camera every 6 – 7 minutes with at 2×2 binning. Exposure time for each channel is 25–50 ms for DAPI; 150 – 250 ms for CFP; 150 – 250 ms for YFP; 500 – 750 ms for Sapphire; 500 – 750 ms for GFP; 300 – 500 ms for Cherry and 300 – 500 ms for Cy5.

Single cell detection of ROS

Cells were stained with CellROX-DeepRed (10422, Invitrogen) at 10 μM for 30 minutes prior to further perturbation. The dye was maintained in culture for the entirety of the experiment. Live cell analysis revealed that the CellROX dye never saturated, even after 6 hours of incubation (data not shown). To account for this, the intensity accumulation rate was incorporated into ROS concentration measurements for each experimental condition.

Image processing

After background subtraction and flat field correction, imaging data were processed to segment and average pixels within each identified cell's nucleus and cytoplasm, using a custom procedure written for MATLAB[26], with modifications in the cytosolic identification protocol as described below. Image data were stored in ND2 files generated by NIS Elements and accessed using the Bio-Formats MATLAB toolbox. Individual cells were tracked over time using uTrack 2.0[27]. Cytoplasmic masks were created by the watershed method[28], and the cytosolic area was further restricted to the area within 5 pixels from the nuclear border. The resulting single-cell time series traces were filtered for quality by a minimum length of trace and maximum number of contiguous missing or corrupt data points.

Imaging and statistical analysis

For all microscopy experiments shown, a minimum of 300 cells were imaged and tracked (in the case of live cell analyses) for each condition. Unless noted otherwise, where single-cell recordings are shown, the displayed cells were chosen by random number generation in MATLAB with a threshold for minimum tracking time to eliminate cells in which the recording was terminated prematurely due to failure of the tracking algorithm. The

Author Manuscript Author Manuscript Author Manuscript Author Manuscript

chosen tracks were manually verified to be representative of successfully tracked cells and consistent with the overall range of cell behaviors. Cell recordings determined by manual inspection to have poor tracking or quantification accuracy were discarded. To determine statistical significance, ANOVA2 was used with Tukey's post hoc analysis, with alpha equal to 0.05. All asterisk symbols indicate p-values less than 0.05.

Flow cytometry

Cells were incubated with 1μM LysoTracker Red DND-99 (L7528, Invitrogen) for 15 minutes and sorted using a Becton-Dickson Fortessa flow cytometer according to published methods[29]. Dead cells were excluded from analysis by 1μg/mL DAPI (D9542, Sigma Aldrich) staining. FlowJo software was used to analyze 20,000 events per run.

Galectin Translocation Assay

MCF7, MDA-MB-231, or NDL cells on glass coverslips in 12 well plates were grown to 70–80% confluency and pre-treated with control (anhydrous methanol), 100μM 1,2-dioleoyl-sn-glycero-3-phospho-(1'-rac-glycerol) (referred to here as 18:1 PG; #840475, Avanti Polar Lipids, Alabaster, AL, USA), or 100μM 1,2-didocosahexaenoyl-sn-glycero-3-[phospho-rac-(1-glycerol)] (referred to here as 22:6 PG; #840492, Avanti) as bovine serum albumin adducts for 1hr, and then treated with vehicle (DMSO) or 10μM FINO2 (25096, Cayman) for 8hr together with lipids. Cells were then fixed with 4% paraformaldehyde for 10min and galectin-3 translocation was evaluated as previously described[30]. Samples were incubated with 50mM ammonium chloride in PBS for 10min, washed three times with PBS, and then permeabilized and blocked in 1 mL blocking buffer (1% BSA, 0.2% NP-40, 5% goat serum, 0.02% sodium azide,) at room temperature for 1hr. Cells were incubated with purified mouse anti-human Galectin-3 (1:100 dilution, #556904, BD Biosciences) diluted in blocking buffer for 1hr at room temperature. Cells were washed three times with PBS and then incubated with goat anti-mouse IgG1 cross-absorbed secondary antibody AlexaFluor 488 conjugate (1:1,000; #A-21121, Invitrogen) at room temperature for 1hr. Cells were again washed three times with PBS before incubation with DAPI (1:10,000) in PBS for 10min in the dark and then rinsed twice with PBS twice before mounting with Fluoromount G. Slides were imaged by confocal microscopy using a ZEISS LSM 800 with Airyscan, and galectin-3 puncta formation was analyzed from ten random fields from three biological replicates with FIJI (https://imagej.net/Fiji) software.

Generation of NDL *mice*

All animal experimental protocols were approved by the Institutional Animal Care and Use Committee (IACUC) of the University of California, Davis, USA. The MMTV-NDL mouse model has previously been described[31]. Wild type FVB-nJ females were crossed with NDL males to generate wild type (WT) and NDL mice, and genotypes were confirmed using polymerase chain reaction using primers for NDL (Fwd-TTC CGG AAC CCA CAT CAG; Rvs- GTT TCC TGC AGC AGC CTA).

Author Manuscript Author Manuscript Author Manuscript Author Manuscript

Mouse Mammary Tumor Monitoring, Tissue Harvesting, and Cell Isolation

Mammary tumors were palpated weekly in female NDL mice commencing at 12 weeks of age, as tumors form spontaneously in multiple mammary glands at approximately 20 weeks of age in the NDL model[31]. NDL female mice were euthanized when the largest tumor reached 10–15mm in diameter, and all tumors were collected, bisected, and immediately snap-frozen. Age-matched WT females were concurrently euthanized, and mammary gland, brain, kidney, liver, lung, spleen, and uterus tissues were harvested and snap-frozen.

For primary cell analyses, fresh NDL mouse tumor and WT mouse mammary gland (pooled per animal) tissues were dissociated into single cells and enriched for the epithelial cell population as previously described[32,33] with minor modifications.

Untargeted lipidomic analysis

1 million cells (cultured and primary) or 5 mg of tissue were extracted with 225 μl of methanol at −20°C containing an internal standard mixture of PE(17:0/17:0), PG(17:0/17:0), PC(17:0/0:0), C17 sphingosine, ceramide (d18:1/17:0), SM (d18:0/17:0), palmitic acid-d_3, PC (12:0/13:0), cholesterol-d_7, TG (17:0/17:1/17:0)-d_5, DG (12:0/12:0/0:0), DG (18:1/2:0/0:0), MG (17:0/0:0/0:0), PE (17:1/0:0), LPC (17:0), LPE (17:1), and 750 μL of MTBE (methyl tertiary butyl ether) (Sigma Aldrich) at −20°C containing the internal standard cholesterol ester 22:1. Because of unavailability, BMP internal standards were not employed. Cells were vortexed for 20 sec, sonicated for 5 min and shaken for 6 min at 4°C with an Orbital Mixing Chilling/Heating Plate (Torrey Pines Scientific Instruments). Then 188 μl of LC-MS grade water (Fisher) was added, samples were vortexed, and centrifuged at 14,000 rcf (Eppendorf 5415D). The upper (non-polar, organic) phase was collected in two 350 μL aliquots and evaporated to dryness. One organic phase aliquot was re-suspended in 100 μL of methanol:toluene (9:1, v/v) mixture containing 50 ng/mL CUDA ((12-[[(cyclohexylamino)carbonyl]amino]-dodecanoic acid) (Cayman Chemical). Samples were then vortexed, sonicated for 5 min and centrifuged at 16,000 rcf and prepared for lipidomic analysis. Method blanks and pooled human plasma (BioreclamationIVT) were included as quality control samples.

Chromatographic and mass spectrometric conditions for lipidomic RPLC-QEHF analysis

Using a ThermoFisher Scientific Vanquish UHPLC system, re-suspended samples were injected at 3 μL and 5 μL for positive and negative electrospray (ESI) modes, respectively, onto a Waters Acquity UPLC CSH C18 (100 mm length × 2.1 mm id; 1.7 μm particle size) with CSH C18 pre-column (5 mm × 2.1 mm id; 1.7 μm particle size). The column was maintained at 65°C. To improve lipid coverage, different mobile phase modifiers were used for positive and negative ESI mode analysis[34]. For positive ESI mode, 10 mM ammonium formate and 0.1% formic acid were used; for negative ESI mode, 10 mM ammonium acetate (Sigma–Aldrich) was employed. Both positive and negative ESI modes used the same mobile phase composition of (A) 60:40 v/v acetonitrile:water (LC-MS grade) and (B) 90:10 v/v isopropanol:acetonitrile. The gradient started at 0 min with 15% (B), 0–2 min 30% (B), 2–2.5 min 48% (B), 2.5–11 min 82% (B), 11–11.5 min 99% (B), 11.5–12 min 99% (B), 12–12.1 min 15% (B), and 12.1–15 min 15% (B). A flow rate of 0.6 mL/min was used. For data acquisition, a Q-Exactive HF Hybrid Quadrupole-Orbitrap Mass Spectrometer was

Author Manuscript Author Manuscript Author Manuscript Author Manuscript

used with the following parameters: mass range, *m/z* 100–1200; MS^1 resolution 60,000: data-dependent MS^2 resolution 15,000; NCE 20, 30, 40; 4 targets/MS^1 scan; gas temperature 369°C, sheath gas flow (nitrogen), 60 units, aux gas flow 25 units, sweep gas flow 2 units; spray voltage 3.59 kV.

LC-MS data processing using MS-DIAL and statistics

Untargeted lipidomic data processing was performed using MS-DIAL[35] for deconvolution, peak picking, alignment, and identification. In house *m/z* and retention time libraries were used in addition to MS/MS spectra databases in msp format[36]. Detected lipids were used for statistical analysis when they were positively detected in at least 50% of all samples in each group. Data were normalized by the sum-norm of all identified lipids (mTIC)[37], to scale each sample. Normalized peak heights were then submitted to R for statistical analysis. Significance was determined by ANOVA analysis with FDR correction and post hoc testing, or *t*-test with Benjamini Hochberg correction.

Results

BMP is enriched in breast cancer cell lysosomes

BMP localization to late endosomal and lysosomal intraluminal vesicles was first established in baby hamster kidney cells using immunofluorescence techniques following development of an anti-BMP/LBPA monoclonal antibody[38]. Here we employed this method to evaluate BMP localization in an array of human breast cancer-derived cell lines as well as non-transformed cells. Breast cancer is a heterogeneous disease; breast cancer subtypes (luminal or basal; estrogen/progesterone receptor positive [ER/PR+], HER2 amplified [HER2+], receptor negative [ER/PR/HER2-]) are phenotypically distinct and each display unique biological properties and malignancy[39]. Our analysis included representatives of each molecular subtype: $ER^-/PR^-/HER2^-$ MDA-MB-231, ER^+/PR^+ MCF7, and $HER2^+$ SKBR3 human breast cancer cell lines, as well the MCF10A human breast epithelial cell line, a commonly utilized non-transformed breast cell model (Supplementary Table S1). Cells were co-labeled with antibodies directed against BMP and lysosome associated membrane protein-1 (LAMP-1), an established lysosome marker protein that, along with LAMP-2, constitutes nearly 50% of total lysosomal membrane protein content and distinguishes lysosomes from their endosomal precursors[40]. Confocal fluorescence microscopy revealed significant overlap of fluorescent signals (Figure 1), with relative quantities variable across cell lines. Likewise, BMP partially co-localizes with Rab7, a late endosome marker[41] (Supplementary Figure S1). These results demonstrate that BMP co-localizes to both breast cancer and non-transformed cell endolysosomal systems, consistent with prior observations with other cell types[38,42].

BMP levels are reduced in breast cancer cells relative to non-tumorigenic cells

Untargeted lipidomic analysis of total BMP levels across human-derived cancer cell lines relative to non-transformed cells revealed a dramatic loss of total BMP abundance with malignant transformation. Total BMP content for each sample was calculated by summing peak intensities reported for each BMP species measured using LC-high resolution MS/MS. BMPs were annotated based upon MS/MS fragmentation using MS-DIAL[35,43] in ESI (+)

Author Manuscript Author Manuscript Author Manuscript Author Manuscript

mode. Separation of phosphatidylglycerol and BMP isomeric species was confirmed using internal standards by MS/MS and retention time matching, indicating effective resolution of these compounds with our chromatography method. Only BMP species with confirmed MS/MS spectra were included in the results for this study.

We observed that BMP levels per cell were highest in normal epithelial MCF10A cells and comparatively low in tumorigenic MDA-MB-231, MCF7, and SKBR3 cell lines, with SKBR3 cells exhibiting lowest abundance (Figure 2A). Notably, total cellular content of phosphatidylcholine (PC) (Figure 2C), the most abundant phospholipid in animal tissues, was roughly constant across all cell lines, though SKBR3 cells exhibited a modest (~17%) elevation in PC content (Figure 2C). This observation suggests that suppressed BMP levels are not secondary to alterations in overall lipid content. Moreover, BMP phosphatidylglycerol (PG) was not reproducibly lower in tumor cells relative to normal (Figure 2B), suggesting that BMP loss does not result from suppressed levels of its presumed precursor.

BMP abundance does not directly correlate with lysosomal content

Previous studies point to BMPs as potential biomarkers for lysosomal storage diseases, likely reflecting enlargement of the lysosome compartment[19]. By quantifying lysosomal content across cell lines, we investigated whether BMP levels are uniquely altered as a result of malignant transformation as opposed to simply correlating with lysosomal content. Consistent with a body of literature describing transformation-associated organelle expansion and upregulation of lysosome biogenesis[22], we observed increased total cellular content of acidic organelles stained with LysoTracker Red in all cancer cell lines (MDA-MB-231, MCF7, and SKBR3) relative to normal MCF10A cells by time-lapse wide-field fluorescent microscopy (Figures 3A and 3B). By comparison, our lipidomics analysis of BMP levels in these cell lines revealed an inverse relationship between the cancer and normal phenotypes. These observations indicate that BMP levels do not correlate with lysosomal content and bolster our hypothesis that the shift in BMP levels detected from normal to cancer cells may reflect a functional role for BMP alteration in transformation.

Transformation alters BMP fatty acid composition in human cell line models

Using our untargeted lipidomics approach, we identified 11 distinct BMP species, allowing us to characterize BMP composition changes across cell lines and detect significant cancer-specific differences in fatty acid chain length and saturation. We observed a striking enrichment of long chain, unsaturated BMPs, particularly DHA (FA 22:6)-containing BMPs, across the molecular subtypes of breast cancer relative to non-transformed cells. Evaluating the abundance of individual BMP species (Supplementary Figure S2), we found that shorter, saturated fatty acyl chain-containing BMPs including the major BMP species 18:1/18:1 accumulated in MCF10A cells (Figure 4A), whereas long, polyunsaturated fatty acyl chains selectively incorporated into cancer cell BMPs, exemplified by BMP 22:6/22:6 elevation across cancer cell lines (MDA-MB-231, MCF7, and SKBR3; Figure 4B). Although MCF10A normal mammary epithelial cells exhibited the highest levels of pooled BMPs in our total abundance analysis, transformed human breast cancer cells displayed significant increases in BMP species consisting of at least one DHA (FA 22:6)

Author Manuscript Author Manuscript Author Manuscript Author Manuscript

acyl chain (Figure 4C). Notably, our analysis revealed an approximate order of magnitude difference in 22:6-containing BMPs between cancer cells and normal cells.

Distribution of DHA (FA 22:6)-containing BMP species in mouse tissues

To evaluate whether our BMP findings in cancer cell lines are relevant *in vivo*, we utilized the well-characterized MMTV-NDL transgenic mouse model of mammary carcinoma. Tumorigenesis in this ERBB2 (HER2)-driven model is driven by an activated rat *c-erbB2/neu* allele (Neu DeLetion mutant, NDL) transgene under the control of the mouse mammary tumor virus promoter (MMTV) in genetically homogeneous FvB/nJ strain mice. Animals spontaneously develop multifocal metastatic adenocarcinomas at approximately 20–24 weeks of age[44,45]. MMTV-NDL tumors and normal mammary gland, brain, kidney, liver, lung, spleen, and uterine tissues from age-matched FVB-nJ mice were harvested and cryopreserved prior to homogenization and total lipid extraction. We analyzed 22:6 fatty acyl chain distribution by lipidomics and observed variable 22:6-containing BMP enrichment across the eight tissues profiled (Figure 5A), with variable BMP species abundance across tissues based on peak height evaluation (Supplementary Figure S3). We found 22:6-containing BMPs to be most highly enriched in brain tissues, likely because DHA is the most abundant PUFA in the brain[46]. Importantly, the 22:6 BMP fraction was dramatically elevated in tumor tissue relative to mammary gland tissue (Figure 5B) in accordance with our findings in human cell lines. Thus, tumor cells may turn on a pathway utilized extensively in tissues such as brain to incorporate the 22:6 fatty acid into BMP.

In an effort to rigorously evaluate whether BMP fatty acid composition might merely be reflective of fatty acid availability, we analyzed the percentage of the 807 tumor lipid species identified that contained at least one esterified 22:6 acyl chain (Figure 5C). The relative frequency of DHA incorporation into total tumor lipids was extremely low (3%) when compared to total BMPs (67.6%), pointing to a regulated and transformation-specific pathway for the incorporation of cellular DHA into BMP lipids.

Tumor cells are enriched in DHA (FA 22:6)-containing BMPs in vivo

Considering the complexity and cellular heterogeneity of mammary tissue, we purified mouse mammary tumor cells and normal mammary epithelial cells for further lipidomics analysis. Tumor cells were harvested from MMTV-NDL tumors, while FVB-nJ mammary glands were dissociated for isolation of the epithelial cell population, as carcinomas originate from the malignant transformation of epithelial cells[44,47]. While non-22:6 fatty acyl chain substituents were comparably distributed in mammary epithelial and tumor cell BMP species (Figure 6A and Supplementary Figure S3), DHA-containing BMPs were significantly elevated in tumor cells relative to non-transformed mammary epithelial cells (Figure 6B and Supplementary Figure S4). Analysis of DHA/22:6-containing BMP species as a percentage of total BMPs again revealed a transformation-specific increase in DHA frequency (Figure 6C), consistent with our findings in human cell lines and animal tissues.

Author Manuscript Author Manuscript Author Manuscript Author Manuscript

DHA-containing BMP precursors scavenge cellular ROS and protect cells from lysosomal membrane permeabilization

We sought to determine the functional relevance of the striking transformation-specific FA 22:6 enrichment in BMPs observed across cell and tissue models in our lipidomics studies. *In vitro* analyses have demonstrated that cellular BMP levels increase following esterified fatty acid supplementation in the form of BMP precursor PG as well as non-esterified FA supplementation[18]. Moreover, supplementation with 22:6-containing PG species promoted accumulation of 22:6-enriched BMP, revealing that BMP fatty acyl chain composition can be manipulated by altering cellular PG reservoirs. Based on findings in macrophages that fatty acyl chain composition dictates BMP stability and sensitivity to oxidative stress-induced degradation[18], and considering that transformation is associated with elevated basal oxidative stress[48], we investigated whether artificially altering BMP composition impacts endogenous ROS in cancer cells. Following supplementation with increasing concentrations of 22:6 PG, we observed significant dose-dependent reductions in cellular ROS levels as determined by single-cell time-lapse imaging of the fluorescent ROS detector CellROX (Figure 7A and 7B). Lipid-mediated ROS buffering was consistent across cell lines, suggesting that FA 22:6 species may function as effective ROS scavengers.

Moreover, using a galectin relocalization assay where cytosolic and nuclear galectin protein relocalizes to punctate structures when lysosomes become permeabilized (Figure 7C)[30], we observed that 20μM and 100μM 22:6 PG but not 18:1 PG rescues cells from lysosomal membrane permeabilization by the LMP-inducing oxidant $FINO_2$ (Figure 7D)[49]. No evidence of cytotoxicity with added lipids was observed. Together, these observations point to the possibility that transformed cells divert PUFAs into BMP for lysosome delivery as a mechanism to preserve organelle integrity in the face of oxidative stress.

Discussion

Presented here is the first comprehensive characterization of BMP in breast cancer, distinguished further by use of untargeted lipidomics methods not previously applied in analyses of BMP in other systems. We profiled BMP species across cell and tissue models and identified a consistent cancer-specific increase in the percentage of 22:6-containing BMPs. Indeed, BMP lipid diversity with regard to structure and abundance has been linked to physiological and pathological processes in other models, suggesting distinct biological functions for these species.

We utilized both antibody-based detection and mass spectrometry techniques to evaluate multiple properties of BMP, from cellular localization to structure and abundance. Immunofluorescence staining demonstrated BMP co-localization with the lysosomal marker LAMP-1 in human-derived cell lines and revealed unsurprising heterogeneity across cancer cell subtypes with regard to lysosome size and distribution based on LAMP-1 signal. Lysosomes cannot be readily distinguished from endosomes based on uniform morphological criteria[50]. While LAMP-1 is canonically utilized as a lysosome-specific marker and is generally overexpressed upon cellular transformation as a consequence of organelle expansion[51–54], LAMP-1 itself can be highly dysregulated in cancers, as evidenced by studies reporting decreased expression after fibroblast transformation[55]. In our

Author Manuscript Author Manuscript Author Manuscript Author Manuscript

studies, we observed a marked LAMP-1 elevation in the highly aggressive ER/PR/HER2- cell line MDA-MB-231, consistent with previous reports that LAMP-1 expression correlates with poor prognosis in breast cancer patients[56].

To achieve sensitive detection of BMP abundance, we analyzed the lipid fraction extracted from human breast cancer and non-transformed mammary epithelial cell lines by mass spectrometry. We observed a dramatic reduction in total BMP levels in cancer cells, which did not correlate with diffrerences in either total cellular lipid content as represented by PC abundance or with PG precursor abundance. This finding suggests that BMPs are specifically suppressed during malignant transformation. BMPs are important in regulating the stability and function of lysosomes, which are adapted upon malignant transformation to maintain survival of cancer cells under physical and mechanical stress[22,57]. We therefore surmise that loss of BMP could selectively sensitize cancer cell lysosomes to rupture by endogenous or exogenous triggers[23]. This mechanism may present an opportunity for therapeutic intervention. For example, drug-induced dissociation of acid sphingomyelinase from its critical cofactor BMP has been demonstrated to disrupt lipid metabolism and to cause lysosomal membrane permeabilization and cell death in breast cancer models[7]. Likewise, we propose that lysosome-targeting agents such as some cationic amphiphilc drugs[58,59] could selectively suppress BMPs in tumor cells to beneath thresholds necessary to maitain cellular viability, leading to cancer-specific cytotoxicity.

Considering previous findings that BMP is a marker for phospholipidosis and LSDs[19,60–62] , we rigorously evaluated lysosomal content across human cell lines by both qualitative and quantitative analysis of LysoTracker Red staining. LysoTracker Red specifically accumulates in acidic structures for effective lysosome labeling[63]. While lysosomes generally measure less than 1 μm in diameter, it is well documented that the lysosome compartment expands with cellular transformation and is more frequently enlarged in aggressive, metastatic cancer cell types[22,64]. Accordingly, our imaging analysis revealed that LysoTracker Red-labeled structures were least abundant in normal MCF10A cells and greatest in invasive MDA-MB-231 cancer cells.

BMP species are highly structurally diverse and reported to be differentially regulated in various disease pathologies[18,60,65,66], suggesting that BMP acyl chain composition may dictate function. Thus, we sought to characterize BMP composition changes in malignancy. We observed an increase in the percentage of FA 22:6 in BMPs across breast cancer cell lines of varying molecular subtype relative to non-transformed mammary epithelial cells. This trend was conserved *in vivo* upon analysis of tumor and mammary gland tissues derived from the commonly utilized genetically modified MMTV-NDL mouse model of mammary tumorigenesis. Comparison of the FA 22:6 fraction in BMPs versus total lipids highlighted a tumor-specific enrichment of 22:6 in BMP that was not simply a consequence of overall fatty acid availability. Our profiling of BMP composition in various non-transformed tissues further highlighted an active regulation of these lipid species across tissues, in line with observations of tissue-specific BMP remodeling in response to metabolic challenge[67]. While total BMP abundance was low in whole mammary gland extracts, this finding was most likely attributed to the low density of epithelial cells in these fatty tissues. For confirmation, we purified tumor cells as well as mammary epithelial cells from

Author Manuscript Author Manuscript Author Manuscript Author Manuscript

mouse mammary glands and measured BMP by lipidomics, which allowed a more direct comparison of transformed tumor cells to their cells of origin than analysis of whole tissues by weight. While some differences were noted in the behaviors of specific BMP species, we again found that cancer cell BMPs were enriched in 22:6 fatty acyl composition. These observations validate our findings in human cells and animal tissues and further illuminating a specific and regulated incorporation of these fatty acyl sidechains into BMPs in cancer.

While few studies have directly addressed the biological significance of BMP fatty acyl chain diversity or assessed functional outcomes of FA 22:6 enrichment found in certain physiological and disease contexts, Bouvier *et al.* discovered that FA 22:6 incorporation into BMP dramatically sensitized BMP to peroxidation[18]. In their studies, macrophage supplementation with BMP's endogenous precursor PG led to specific elevation of BMP levels relative to other phospholipids[18]. Moreover, supplementation with 22:6/22:6- or 18:1/18:1-PG selectively augmented the 22:6- or 18:1-containing BMP fraction, respectively, with 22:6 PG-supplemented cells demonstrating a loss of total BMP content when exposed to oxidative stress[18]. In contrast, BMP levels were unaffected in 18:1 PG supplemented cells. As cancer cells display elevated levels of basal oxidant stress[48], we hypothesized that a transformation-associated stress response may underlie the enhanced propensity for cancer cell BMPs to accumulate 22:6 as revealed by our lipidomics studies. Indeed, we observed a dramatic reduction in endogenous ROS with supplementation of increasing 22:6 PG concentrations. It is possible, as initially suggested by Bouvier *et al.*[18], that 22:6-enriched BMP species function as local antioxidants. Lysosomes contain major cellular reservoirs of chelatable iron that can catalyze Fenton reactions in redox cycling to produce ROS. Drug-induced iron sequestration led to ROS-mediated lysosomal rupture and breast cancer ferroptotic stem cell death in a recent study[68], signifying the importance of ROS scavenging in the maintenance of lysosomal membrane stability. Thus, it is noteworthy that our studies show that 22:6 PG but not 18:1 PG rescue breast cancer cells from oxidant-induced LMP, raising the possibility that PUFA-rich BMPs may suppress the cellular cytotoxicity associated with elevated ROS in tumor cells. Further assessment of differential BMP peroxidation and characterization of oxidized BMP forms, requiring advancement of our mass spectrometry analytical methods, are required to fully elucidate 22:6 BMP activity in lysosomal ROS scavenging, and furthermore, how that may dynamically interplay with BMP as it operates in maintenance of organelle structure and function.

Overall, our observations are consistent with a working model whereby transformed cells divert PUFAs into BMP as an adaptive response to the elevated ROS levels associated cancer. Because BMPs are specifically delivered to the lysosome interior via luminal vesicles, they may serve as very efficient shuttles for the delivery for the delivery of fatty acid antioxidants. In this model, the observed suppressed levels of BMPs in tumors may be secondary to their oxidation and subsequent breakdown rather than to altered metabolic processing. Nonetheless, suppressed BMP levels could lead to blunted lysosomal sphingolipid breakdown and accumulation of sphingolipid species within lysosomes, and the increased fragility of the limiting lysosomal membrane characteristic of transformed cells. Further studies will be necessary to confirm this model and discern the underlying mechanisms of BMP suppression and PUFA incorporation.

Author Manuscript Author Manuscript Author Manuscript Author Manuscript

Supplementary Material

Refer to Web version on PubMed Central for supplementary material.

Acknowledgments

This work was funded by NIH U2C ES030158 (OF) and NIH CA250211 (KLC).

Abbreviations:

BMP	bis(monoacylglycerol)phosphate
CFP	cyan fluorescence protein
DHA	docosahexaenoic acid (22:6)
FA	fatty acid
GFP	green fluorescence protein
LBPA	lysobisphosphatidic acid
LMP	lysosomal membrane permeabilization
LSD	lysosomal storage disease
PBS	phosphate-buffered saline
PG	phosphatidyglycerol
PUFA	polyunsaturated fatty acid
ROS	reactive oxygen species
YFP	yellow fluorescence protein

References

1. Body DR, Gray GM 1967. The isolation and characterisation of phosphatidylglycerol and a structural isomer from pig lung. Chem Phys Lipids 1, 254–263. 10.1016/0009-3084(67)90032-1
2. Showalter MR, Berg AL, Nagourney A, Heil H, Carraway KL 3rd, Fiehn O. 2020. The emerging and diverse roles of bis(monoacylglycero) phosphate lipids in cellular physiology and disease. Int J Mol Sci 21, 21. 10.3390/ijms21218067
3. Schulze H, Sandhoff K, 2011. Lysosomal lipid storage diseases. Cold Spring Harb Perspect Biol 3. 10.1101/cshperspect.a004804
4. Christie WW (2022). Bis(monoacylglycero)phosphate. The Lipid Web. https://www.lipidmaps.org/resources/lipidweb/lipidweb_html/lipids/complex/lysobpa/index.htm
5. Hullin-Matsuda F, Kawasaki K, Delton-Vandenbroucke I, Xu Y, Nishijima M, Lagarde M, Schlame M, Kobayashi T. 2007. De novo biosynthesis of the late endosome lipid, bis(monoacylglycero)phosphate. J Lipid Res 48, 1997–2008. 10.1194/jlr.M700154-JLR200 [PubMed: 17558022]
6. Pribasnig MA, Mrak I, Grabner GF, Taschler U, Knittelfelder O, Scherz B, Eichmann TO, Heier C, Grumet L, Kowaliuk J, Romauch M, Holler S, Anderl F, Wolinski H, Lass A, Breinbauer R, Marsche G, Brown JM, Zimmermann R. 2015. α/β Hydrolase Domain-containing 6 (ABHD6)

Author Manuscript Author Manuscript Author Manuscript Author Manuscript

Degrades the Late Endosomal/Lysosomal Lipid Bis(monoacylglycero)phosphate. J Biol Chem 290, 29869–29881. 10.1074/jbc.M115.669168 [PubMed: 26491015]

7. Petersen NHT, Olsen OD, Groth-Pedersen L, Ellegaard A-M, Bilgin M, Redmer S, Ostenfeld MS, Ulanet D, Dovmark TH, Lønborg A, Vindeløv SD, Hanahan D, Arenz C, Ejsing CS, Kirkegaard T, Rohde M, Nylandsted J, Jäättelä M. 2013. Transformation-associated changes in sphingolipid metabolism sensitize cells to lysosomal cell death induced by inhibitors of acid sphingomyelinase. Cancer Cell 24, 379–393. 10.1016/j.ccr.2013.08.003 [PubMed: 24029234]
8. Kolter T, Sandhoff K, 2010. Lysosomal degradation of membrane lipids. FEBS Lett 584, 1700–1712. 10.1016/j.febslet.2009.10.021 [PubMed: 19836391]
9. Gallala HD, Sandhoff K. 2011. Biological function of the cellular lipid BMP-BMP as a key activator for cholesterol sorting and membrane digestion. Neurochem Res 36, 1594–1600. 10.1007/s11064-010-0337-6 [PubMed: 21136156]
10. Akgoc Z, Iosim S, Seyfried TN 2015. Bis(monoacylglycero)phosphate as a macrophage enriched phospholipid. Lipids 50, 907–912. 10.1007/s11745-015-4045-5 [PubMed: 26205346]
11. Brotherus J, Renkonen O, Fischer W, Herrmann J, 1974. Novel stereoconfiguration in lyso-bis-phosphatidic acid of cultured BHK-cells. Chem Phys Lipids 13, 178–182. 10.1016/0009-3084(74)90034-6 [PubMed: 4473276]
12. Mason RJ, Stossel TP, Vaughan M. 1972. Lipids of alveolar macrophages, polymorphonuclear leukocytes, and their phagocytic vesicles. J Clin Invest 51, 2399–2407. 10.1172/JCI107052 [PubMed: 4344731]
13. Cochran FR, Connor JR, Roddick VL, Waite BM 1985. Lyso(bis)phosphatidic acid: a novel source of arachidonic acid for oxidative metabolism by rabbit alveolar macrophages. Biochem Biophys Res Commun 130, 800–806. 10.1016/0006-291x(85)90487-5 [PubMed: 3927910]
14. Wherrett JR, Huterer S. 1973. Bis-(monoacylglyceryl)-phosphate of rat and human liver: fatty acid composition and NMR spectroscopy. Lipids 8, 531–533. 10.1007/BF02531989 [PubMed: 4743203]
15. Wang M, Palavicini JP, Csereznye A, Han X. 2017. Strategy for quantitative analysis of isomeric bis(monoacylglycero)phosphate and phosphatidylglycerol species by shotgun lipidomics after one-step methylation. Anal Chem 89, 8490–8495. 10.1021/acs.analchem.7b02058 [PubMed: 28708380]
16. Vosse C, Wienken C, Cadenas C, Hayen H. 2018. Separation and identification of phospholipids by hydrophilic interaction liquid chromatography coupled to tandem high resolution mass spectrometry with focus on isomeric phosphatidylglycerol and bis(monoacylglycero)phosphate. J Chromatogr A 1565, 105–113. 10.1016/j.chroma.2018.06.039 [PubMed: 29983166]
17. Rabia M, Leuzy V, Soulage C, Durand A, Fourmaux B, Errazuriz-Cerda E, Köffel R, Draeger A, Colosetti P, Jalabert A, Di Filippo M, Villard-Garon A, Bergerot C, Luquain-Costaz C, Moulin P, Rome S, Delton I, Hullin-Matsuda F, 2020. Bis(monoacylglycero)phosphate, a new lipid signature of endosome-derived extracellular vesicles. Biochimie 178, 26–38. 10.1016/j.biochi.2020.07.005 [PubMed: 32659447]
18. Bouvier J, Zemski Berry KA, Hullin-Matsuda F, Makino A, Michaud S, Geloën A, Murphy RC, Kobayashi T, Lagarde M, Delton-Vandenbroucke I. 2009. Selective decrease of bis(monoacylglycero)phosphate content in macrophages by high supplementation with docosahexaenoic acid. J Lipid Res 50, 243–255. 10.1194/jlr.M800300-JLR200 [PubMed: 18809971]
19. Meikle PJ, Duplock S, Blacklock D, Whitfield PD, Macintosh G, Hopwood JJ, Fuller M. 2008. Effect of lysosomal storage on bis(monoacylglycero)phosphate. Biochem J 411, 71–78. 10.1042/BJ20071043 [PubMed: 18052935]
20. Hein LK, Duplock S, Fuller M. 2013. Selective reduction of bis(monoacylglycero)phosphate ameliorates the storage burden in a THP-1 macrophage model of Gaucher disease. J Lipid Res 54, 1691–1697. 10.1194/jlr.M038232 [PubMed: 23564732]
21. Serrano-Puebla A, Boya P, 2018. Lysosomal membrane permeabilization as a cell death mechanism in cancer cells. Biochem Soc Trans 46, 207–215. 10.1042/BST20170130 [PubMed: 29472365]

Author Manuscript Author Manuscript Author Manuscript Author Manuscript

22. Jäättelä M, Kallunki T. 2016. Lysosome and Cancer. Lysosomes: Biology, Diseases, and Therapeutics, 10.1002/9781118978320.ch10
23. Aits S, Jäättelä M. 2013. Lysosomal cell death at a glance. J Cell Sci 126, 1905–1912. 10.1242/jcs.091181 [PubMed: 23720375]
24. Kallunki T, Olsen OD, Jäättelä M. 2013. Cancer-associated lysosomal changes: friends or foes? Oncogene 32, 1995–2004. 10.1038/onc.2012.292 [PubMed: 22777359]
25. Hung YP, Teragawa C, Kosaisawe N, Gillies TE, Pargett M, Minguet M, Distor K, Rocha-Gregg BL, Coloff JL, Keibler MA, Stephanopoulos G, Yellen G, Brugge JS, Albeck JG 2017. Akt regulation of glycolysis mediates bioenergetic stability in epithelial cells. Elife 6. 10.7554/eLife.27293
26. Pargett M, Gillies TE, Teragawa CK, Sparta B, Albeck JG 2017. Single-cell imaging of ERK signaling using fluorescent biosensors. In Methods in Molecular Biology vol 1636, pp. 35–59. Humana Press Inc. 10.1007/978-1-4939-7154-1_3 [PubMed: 28730471]
27. Jaqaman K, Loerke D, Mettlen M, Kuwata H, Grinstein S, Schmid SL, Danuser G. 2008. Robust single-particle tracking in live-cell time-lapse sequences. Nat Methods 5, 695–702. 10.1038/nmeth.1237 [PubMed: 18641657]
28. Vincent L, Soille P. 1991. Watersheds in digital spaces: an efficient algorithm based on immersion simulations. In IEEE Transactions on Pattern Analysis and Machine Intelligence vol 13, pp. 583–598, 10.1109/34.87344
29. Xiao Q, Yan P, Ma X, Liu H, Perez R, Zhu A, Gonzales E, Burchett JM, Schuler DR, Cirrito JR, Diwan A, Lee J-M 2014. Enhancing astrocytic lysosome biogenesis facilitates Aβ clearance and attenuates amyloid plaque pathogenesis. J Neurosci 34, 9607–9620. 10.1523/JNEUROSCI.3788-13.2014 [PubMed: 25031402]
30. Aits S, Jäättelä M, Nylandsted J. 2015. Methods for the quantification of lysosomal membrane permeabilization: a hallmark of lysosomal cell death. Methods Cell Biol 126, 261–285. 10.1016/bs.mcb.2014.10.032 [PubMed: 25665450]
31. Siegel PM, Ryan ED, Cardiff RD, Muller WJ 1999. Elevated expression of activated forms of Neu/ErbB-2 and ErbB-3 are involved in the induction of mammary tumors in transgenic mice: implications for human breast cancer. EMBO J 18, 2149–2164. 10.1093/emboj/18.8.2149 [PubMed: 10205169]
32. Cho RW, Wang X, Diehn M, Shedden K, Chen GY, Sherlock G, Gurney A, Lewicki J, Clarke MF 2008. Isolation and molecular characterization of cancer stem cells in MMTV-Wnt-1 murine breast tumors. Stem Cells 26, 364–371. 10.1634/stemcells.2007-0440 [PubMed: 17975224]
33. Diehn M, Cho RW, Lobo NA, Kalisky T, Dorie MJ, Kulp AN, Qian D, Lam JS, Ailles LE, Wong M, Joshua B, Kaplan MJ, Wapnir I, Dirbas FM, Somlo G, Garberoglio C, Paz B, Shen J, Lau SK, Quake SR, Brown JM, Weissman IL, Clarke MF 2009. Association of reactive oxygen species levels and radioresistance in cancer stem cells. Nature 458, 780–783. 10.1038/nature07733 [PubMed: 19194462]
34. Cajka T, Fiehn O. 2016. Increasing lipidomic coverage by selecting optimal mobile-phase modifiers in LC–MS of blood plasma. Metabolomics 12, 34. 10.1007/s11306-015-0929-x
35. Tsugawa H, Cajka T, Kind T, Ma Y, Higgins B, Ikeda K, Kanazawa M, VanderGheynst J, Fiehn O, Arita M. 2015. MS-DIAL: data-independent MS/MS deconvolution for comprehensive metabolome analysis. Nat Methods 12, 523–526. 10.1038/nmeth.3393 [PubMed: 25938372]
36. Kind T, Liu K-H, Lee DY, DeFelice B, Meissen JK, Fiehn O. 2013. LipidBlast in silico tandem mass spectrometry database for lipid identification. Nat Methods 10, 755–758. 10.1038/nmeth.2551 [PubMed: 23817071]
37. Fan S, Kind T, Cajka T, Hazen SL, Tang WHW, Kaddurah-Daouk R, Irvin MR, Arnett DK, Barupal DK, Fiehn O. 2019. Systematic Error Removal Using Random Forest for Normalizing Large-Scale Untargeted Lipidomics Data. Anal Chem 91, 3590–3596. 10.1021/acs.analchem.8b05592 [PubMed: 30758187]
38. Kobayashi T, Stang E, Fang KS, de Moerloose P, Parton RG, Gruenberg J. 1998. A lipid associated with the antiphospholipid syndrome regulates endosome structure and function. Nature 392, 193–197. 10.1038/32440 [PubMed: 9515966]

Author Manuscript Author Manuscript Author Manuscript Author Manuscript

39. Kittaneh M, Montero AJ, Glück S. 2013. Molecular profiling for breast cancer: a comprehensive review. Biomark Cancer 5, 61–70. 10.4137/BIC.S9455 [PubMed: 24250234]
40. Wartosch L, Bright NA, Luzio JP 2015. Lysosomes. Curr Biol 25, R315–316. 10.1016/j.cub.2015.02.027 [PubMed: 25898096]
41. Wang T, Ming Z, Xiaochun W, Hong W, 2011. Rab7: role of its protein interaction cascades in endo-lysosomal traffic. Cell Signal 23, 516–521. 10.1016/j.cellsig.2010.09.012 [PubMed: 20851765]
42. Kobayashi T, Beuchat MH, Lindsay M, Frias S, Palmiter RD, Sakuraba H, Parton RG, Gruenberg J. 1999. Late endosomal membranes rich in lysobisphosphatidic acid regulate cholesterol transport. Nat Cell Biol 1, 113–118. 10.1038/10084 [PubMed: 10559883]
43. Tsugawa H, Ikeda K, Takahashi M, Satoh A, Mori Y, Uchino H, Okahashi N, Yamada Y, Tada I, Bonini P, Higashi Y, Okazaki Y, Zhou Z, Zhu Z-J, Koelmel J, Cajka T, Fiehn O, Saito K, Arita Masanori, Arita Makoto, 2020. A lipidome atlas in MS-DIAL 4. Nat Biotechnol 38, 1159–1163. 10.1038/s41587-020-0531-2 [PubMed: 32541957]
44. Guy CT, Webster MA, Schaller M, Parsons TJ, Cardiff RD, Muller WJ 1992. Expression of the neu protooncogene in the mammary epithelium of transgenic mice induces metastatic disease. Proc Natl Acad Sci U S A 89, 10578–10582. 10.1073/pnas.89.22.10578 [PubMed: 1359541]
45. Ingalla EQ, Miller JK, Wald JH, Workman HC, Kaur RP, Yen L, Fry WHD, Borowsky AD, Young LJT, Sweeney C, Carraway KL 3rd, 2010. Post-transcriptional mechanisms contribute to the suppression of the ErbB3 negative regulator protein Nrdp1 in mammary tumors. J Biol Chem 285, 28691–28697. 10.1074/jbc.M110.127977 [PubMed: 20628057]
46. Lacombe RJS, Chouinard-Watkins R, Bazinet RP, 2018. Brain docosahexaenoic acid uptake and metabolism. Mol Aspects Med 64, 109–134. 10.1016/j.mam.2017.12.004 [PubMed: 29305120]
47. Guy CT, Cardiff RD, Muller WJ 1996. Activated neu induces rapid tumor progression. J Biol Chem 271, 7673–7678. 10.1074/jbc.271.13.7673 [PubMed: 8631805]
48. Schumacker PT 2006. Reactive oxygen species in cancer cells: live by the sword, die by the sword. Cancer Cell 10, 175–176. 10.1016/j.ccr.2006.08.015 [PubMed: 16959608]
49. Gaschler MM, Andia AA, Liu H, Csuka JM, Hurlocker B, Vaiana CA, Heindel DW, Zuckerman DS, Bos PH, Reznik E, Ye LF, Tyurina YY, Lin AJ, Shchepinov MS, Chan AY, Peguero-Pereira E, Fomich MA, Daniels JD, Bekish AV, Shmanai VV, Kagan VE, Mahal LK, Woerpel KA, Stockwell BR 2018. FINO(2) initiates ferroptosis through GPX4 inactivation and iron oxidation. Nat Chem Biol 14, 507–515. 10.1038/s41589-018-0031-6 [PubMed: 29610484]
50. de Duve C. 1983. Lysosomes revisited. Eur J Biochem 137, 391–397. 10.1111/j.1432-1033.1983.tb07841.x [PubMed: 6319122]
51. Furuta K, Ikeda M, Nakayama Y, Nakamura K, Tanaka M, Hamasaki N, Himeno M, Hamilton SR, August JT 2001. Expression of lysosome-associated membrane proteins in human colorectal neoplasms and inflammatory diseases. Am J Pathol 159, 449–455. 10.1016/S0002-9440(10)61716-6 [PubMed: 11485903]
52. Ozaki K, Nagata M, Suzuki M, Fujiwara T, Ueda K, Miyoshi Y, Takahashi E, Nakamura Y. 1998. Isolation and characterization of a novel human lung-specific gene homologous to lysosomal membrane glycoproteins 1 and 2: significantly increased expression in cancers of various tissues. Cancer Res 58, 3499–3503. [PubMed: 9721848]
53. Künzli BM, Berberat PO, Zhu ZW, Martignoni M, Kleeff J, Tempia-Caliera AA, Fukuda M, Zimmermann A, Friess H, Büchler MW, 2002. Influences of the lysosomal associated membrane proteins (Lamp-1, Lamp-2) and Mac-2 binding protein (Mac-2-BP) on the prognosis of pancreatic carcinoma. Cancer 94, 228–239. 10.1002/cncr.10162 [PubMed: 11815981]
54. Jensen SS, Aaberg-Jessen C, Christensen KG, Kristensen B, 2013. Expression of the lysosomal-associated membrane protein-1 (LAMP-1) in astrocytomas. Int J Clin Exp Pathol 6, 1294–1305. [PubMed: 23826410]
55. Fehrenbacher N, Bastholm L, Kirkegaard-Sørensen T, Rafn B, Bøttzauw T, Nielsen C, Weber E, Shirasawa S, Kallunki T, Jäättelä M, 2008. Sensitization to the lysosomal cell death pathway by oncogene-induced down-regulation of lysosome-associated membrane proteins 1 and 2. Cancer Res 68, 6623–6633. 10.1158/0008-5472.CAN-08-0463 [PubMed: 18701486]

Author Manuscript Author Manuscript Author Manuscript Author Manuscript

56. Wang Q, Yao J, Jin Q, Wang X, Zhu H, Huang F, Wang W, Qiang J, Ni Q, 2017. LAMP1 expression is associated with poor prognosis in breast cancer. Oncol Lett 14, 4729–4735. 10.3892/ol.2017.6757 [PubMed: 29085473]

57. Northcott JM, Dean IS, Mouw JK, Weaver VM, 2018. Feeling Stress: The Mechanics of Cancer Progression and Aggression. Front Cell Dev Biol 6, 17. 10.3389/fcell.2018.00017 [PubMed: 29541636]

58. Hu M, Carraway KL 3rd, 2020. Repurposing Cationic Amphiphilic Drugs and Derivatives to Engage Lysosomal Cell Death in Cancer Treatment. Front Oncol 10, 605361. 10.3389/fonc.2020.605361 [PubMed: 33425762]

59. Ellegaard A-M, Bach P, Jäättelä M, 2021. Targeting Cancer Lysosomes with Good Old Cationic Amphiphilic Drugs. Rev Physiol Biochem Pharmacol. 10.1007/112_2020_56

60. Liu N, Tengstrand EA, Chourb L, Hsieh FY, 2014. Di-22:6-bis(monoacylglycerol)phosphate: A clinical biomarker of drug-induced phospholipidosis for drug development and safety assessment. Toxicol Appl Pharmacol 279, 467–476. 10.1016/j.taap.2014.06.014 [PubMed: 24967688]

61. Thompson KL, Haskins K, Rosenzweig BA, Stewart S, Zhang J, Peters D, Knapton A, Rouse R, Mans D, Colatsky T, 2012. Comparison of the diagnostic accuracy of di-22:6-bis(monoacylglycerol)phosphate and other urinary phospholipids for drug-induced phospholipidosis or tissue injury in the rat. Int J Toxicol 31, 14–24. 10.1177/1091581811430167 [PubMed: 22267869]

62. Hullin-Matsuda F, Luquain-Costaz C, Bouvier J, Delton-Vandenbroucke I, 2009. Bis(monoacylglycero)phosphate, a peculiar phospholipid to control the fate of cholesterol: Implications in pathology. Prostaglandins Leukot Essent Fatty Acids 81, 313–324. 10.1016/j.plefa.2009.09.006 [PubMed: 19857945]

63. Bampton ETW, Goemans CG, Niranjan D, Mizushima N, Tolkovsky AM, 2005. The dynamics of autophagy visualized in live cells: from autophagosome formation to fusion with endo/lysosomes. Autophagy 1, 23–36. 10.4161/auto.1.1.1495 [PubMed: 16874023]

64. Glunde K, Guggino SE, Solaiyappan M, Pathak AP, Ichikawa Y, Bhujwalla ZM, 2003. Extracellular acidification alters lysosomal trafficking in human breast cancer cells. Neoplasia 5, 533–545. 10.1016/s1476-5586(03)80037-4 [PubMed: 14965446]

65. Thomas G, Betters JL, Lord CC, Brown AL, Marshall S, Ferguson D, Sawyer J, Davis MA, Melchior JT, Blume LC, Howlett AC, Ivanova PT, Milne SB, Myers DS, Mrak I, Leber V, Heier C, Taschler U, Blankman JL, Cravatt BF, Lee RG, Crooke RM, Graham MJ, Zimmermann R, Brown HA, Brown JM, 2013. The serine hydrolase ABHD6 Is a critical regulator of the metabolic syndrome. Cell Rep 5, 508–520. 10.1016/j.celrep.2013.08.047 [PubMed: 24095738]

66. Rampanelli E, Ochodnicky P, Vissers JP, Butter LM, Claessen N, Calcagni A, Kors L, Gethings LA, Bakker SJ, de Borst MH, Navis GJ, Liebisch G, Speijer D, van den Bergh Weerman MA, Jung B, Aten J, Steenbergen E, Schmitz G, Ballabio A, Florquin S, Aerts JM, Leemans JC, 2018. Excessive dietary lipid intake provokes an acquired form of lysosomal lipid storage disease in the kidney. J Pathol 246, 470–484. 10.1002/path.5150 [PubMed: 30073645]

67. Grabner GF, Fawzy N, Schreiber R, Pusch LM, Bulfon D, Koefeler H, Eichmann TO, Lass A, Schweiger M, Marsche G, Schoiswohl G, Taschler U, Zimmermann R, 2020. Metabolic regulation of the lysosomal cofactor bis(monoacylglycero)phosphate in mice. J Lipid Res 61, 995–1003. 10.1194/jlr.RA119000516 [PubMed: 32350080]

68. Mai TT, Hamaï A, Hienzsch A, Cañeque T, Müller S, Wicinski J, Cabaud O, Leroy C, David A, Acevedo V, Ryo A, Ginestier C, Birnbaum D, Charafe-Jauffret E, Codogno P, Mehrpour M, Rodriguez R, 2017. Salinomycin kills cancer stem cells by sequestering iron in lysosomes. Nat Chem 9, 1025–1033. 10.1038/nchem.2778 [PubMed: 28937680]

Author Manuscript Author Manuscript Author Manuscript Author Manuscript

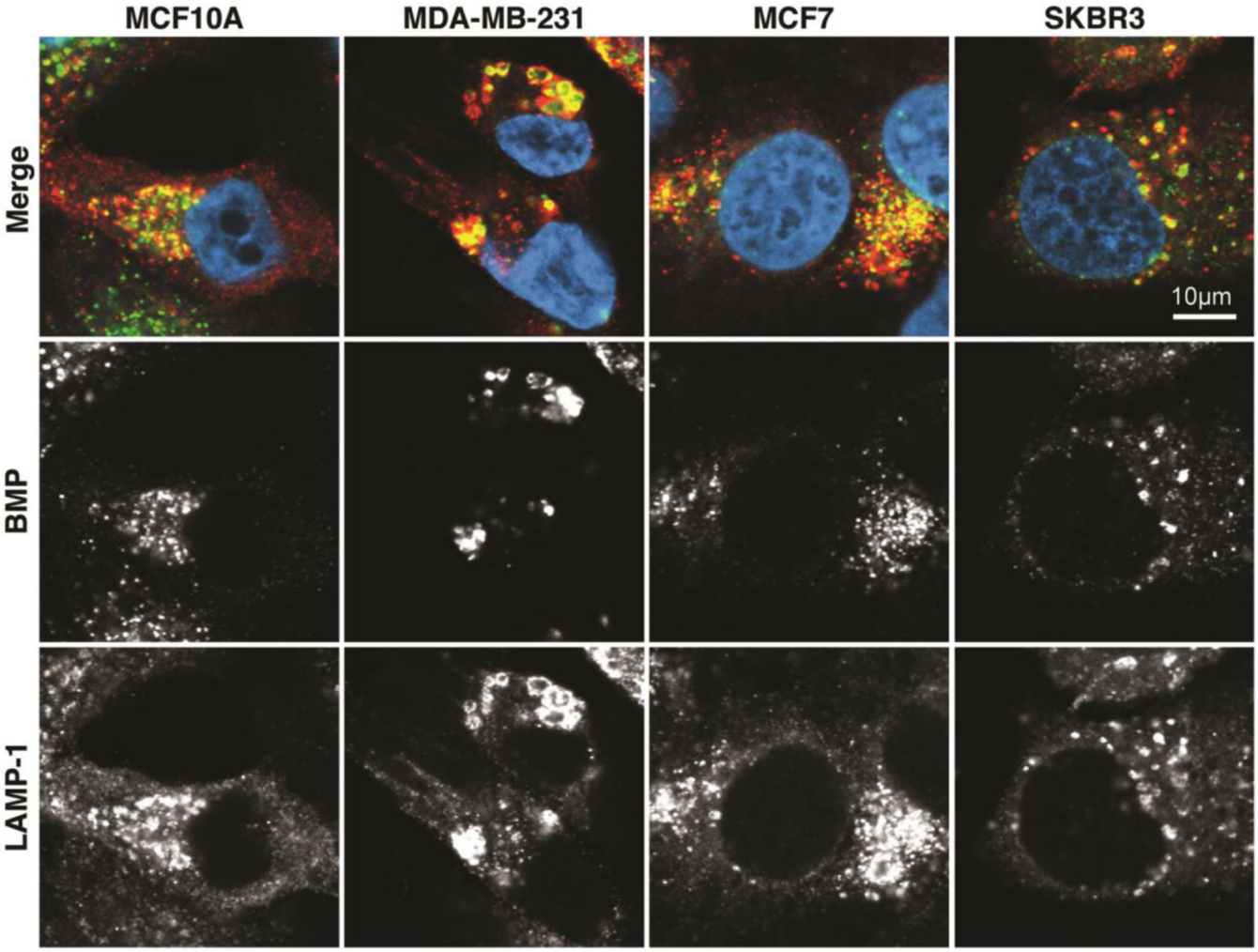

Figure 1. BMP is enriched in lysosomes.

MCF10A, MDA-MB-231, MCF7 and SKBR3 cells were fixed and stained with anti-BMP/LBPA (*green*) and anti-LAMP1 (*red*) antibodies. Nuclei were counterstained with DAPI (*blue*). The appearance of *yellow* staining in confocal microscopic images indicates colocalization. Data are representative of three independent replicate experiments. Scale bar = 10μm.

Author Manuscript Author Manuscript Author Manuscript Author Manuscript

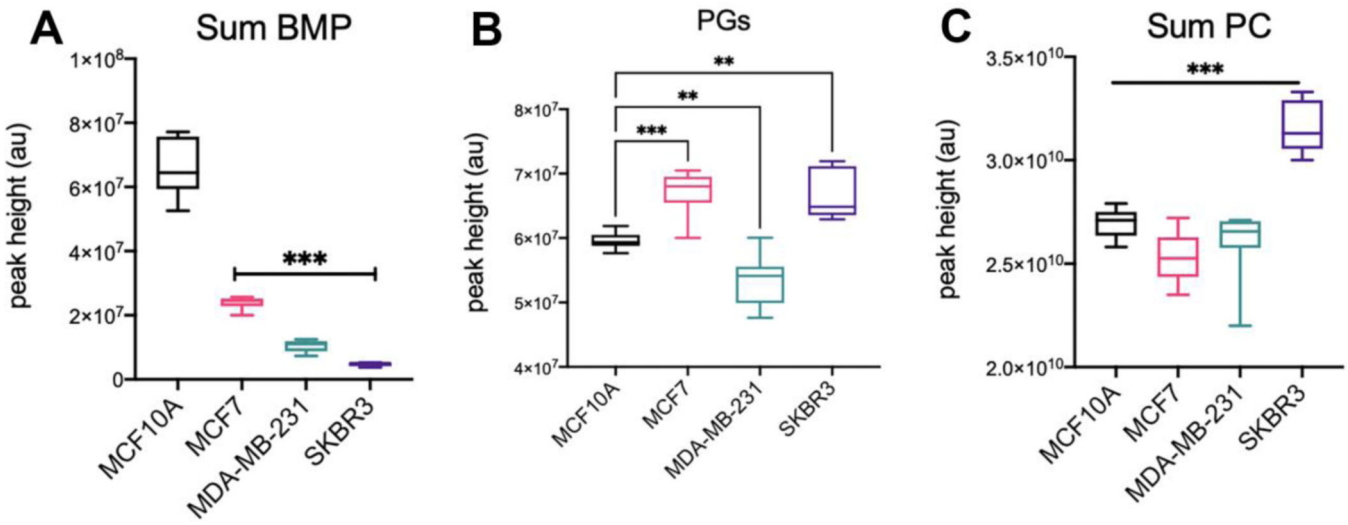

Figure 2. BMPs levels are reduced in cancer cells relative to non-tumorigenic cells.

(A) Mass spectrum peak height data for pooled BMP species isolated from the indicated human breast tumor-derived (MDA-MB-231, MCF7, SKBR3) and normal (MCF10A) cell lines were measured using RPLC-QEHFMS and normalized to cell count. **(B)** Peak heights for pooled PG species indicate that the effect on BMP is not an outcome of precursor availability. **(C)** Peak heights for pooled PC species demonstrate that transformation-associated suppression of BMP levels is not common to all lipid species. In all panels, average peak heights are shown ($n = 10$ replicates of 1 million cells), and box plots for each cell line were drawn using ggplot2 in R statistical program. Significance was determined by ANOVA with Tukey's post-hoc analysis and FDR correction. P values shown here convey significance relative to MCF10A; ***, $P < 0.001$. All P values are presented in Supplementary Table S2.

Author Manuscript Author Manuscript Author Manuscript Author Manuscript

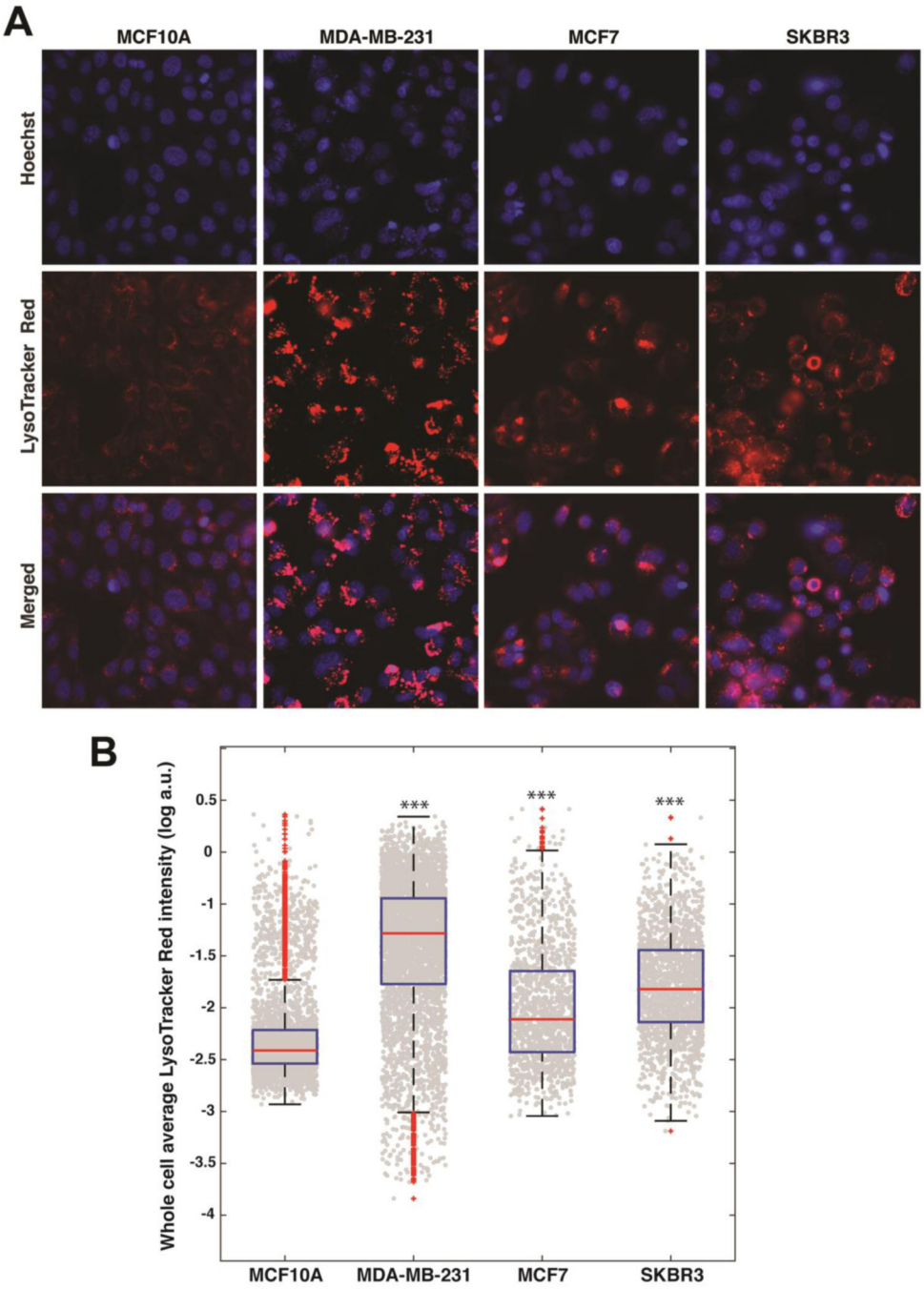

Figure 3. Lysosomal content in human-derived breast cell lines.

Representative images **(A)** and quantitation **(B)** of LysoTracker Red staining in MCF10A, MDA-MB-231, MCF7, and SKBR3 cells. Lysosomes were specifically labeled with 50nM LysoTracker Red (*red*), and signal intensity was analyzed by fluorescence microscopy and normalized to cell count. Nuclei were stained with Hoechst dye (*blue*). Boxes represent the 2nd and 3rd quartiles, while whiskers extend to values 1.5 times the interquartile range (IQR) of the first and third quartiles. Data are representative of three independent imaging

experiments. Significance was determined by ANOVA with Tukey's post-hoc analysis and FDR correction. *P* values convey significance relative to MCF10A; ***, $P < 0.001$.

Author Manuscript Author Manuscript Author Manuscript Author Manuscript

Author Manuscript Author Manuscript Author Manuscript Author Manuscript

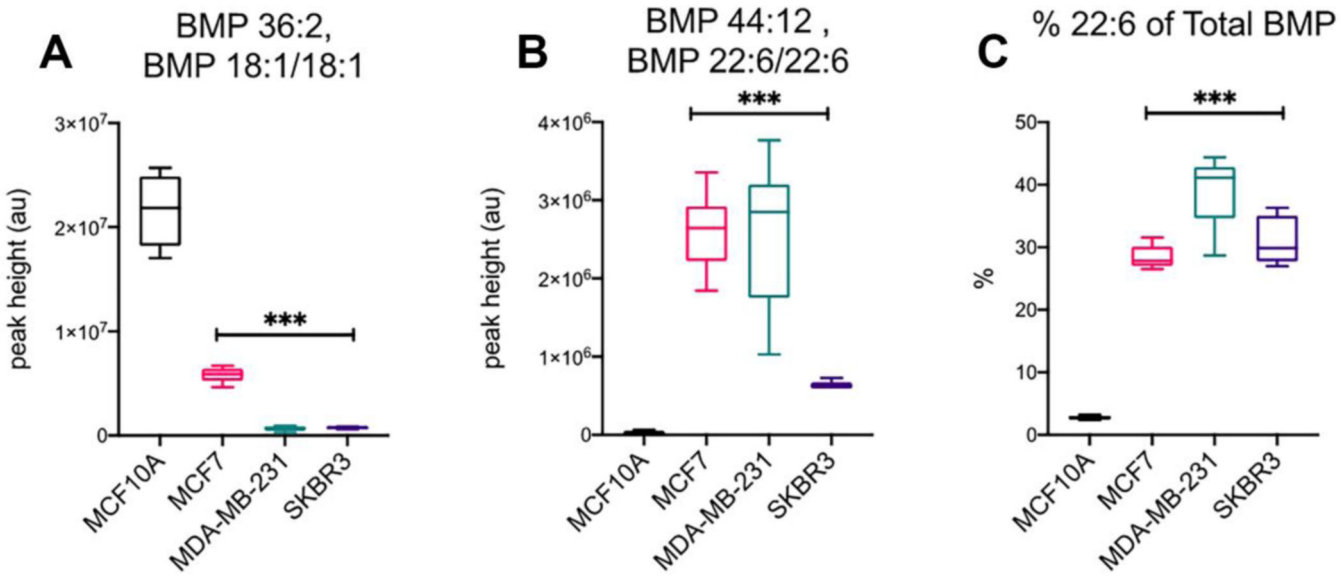

Figure 4. Untargeted lipidomics reveals differential BMP fatty acid composition in cancer versus normal human breast cell lines.

Quantities of di-18:1 **(A)** and di-22:6 **(B)** BMP species are presented as peak height values. **(C)** Levels of BMP species in MCF10A, MDA-MB-231, MCF7 and SKBR3 cell lines were measured using RPLC-QEHFMS, and DHA (FA 22:6)-containing BMPs are expressed as a percentage of total BMP levels. Averages for each compound by cell line are shown (n = 10 replicates of 1 million cells), and box plots were drawn using ggplot2 in R statistical program. Significance was determined by ANOVA with Tukey's post-hoc analysis and FDR correction. P values shown here convey significance relative to MCF10A; $P < 0.001$. All P values are presented in Supplementary Table S2.

Author Manuscript Author Manuscript Author Manuscript Author Manuscript

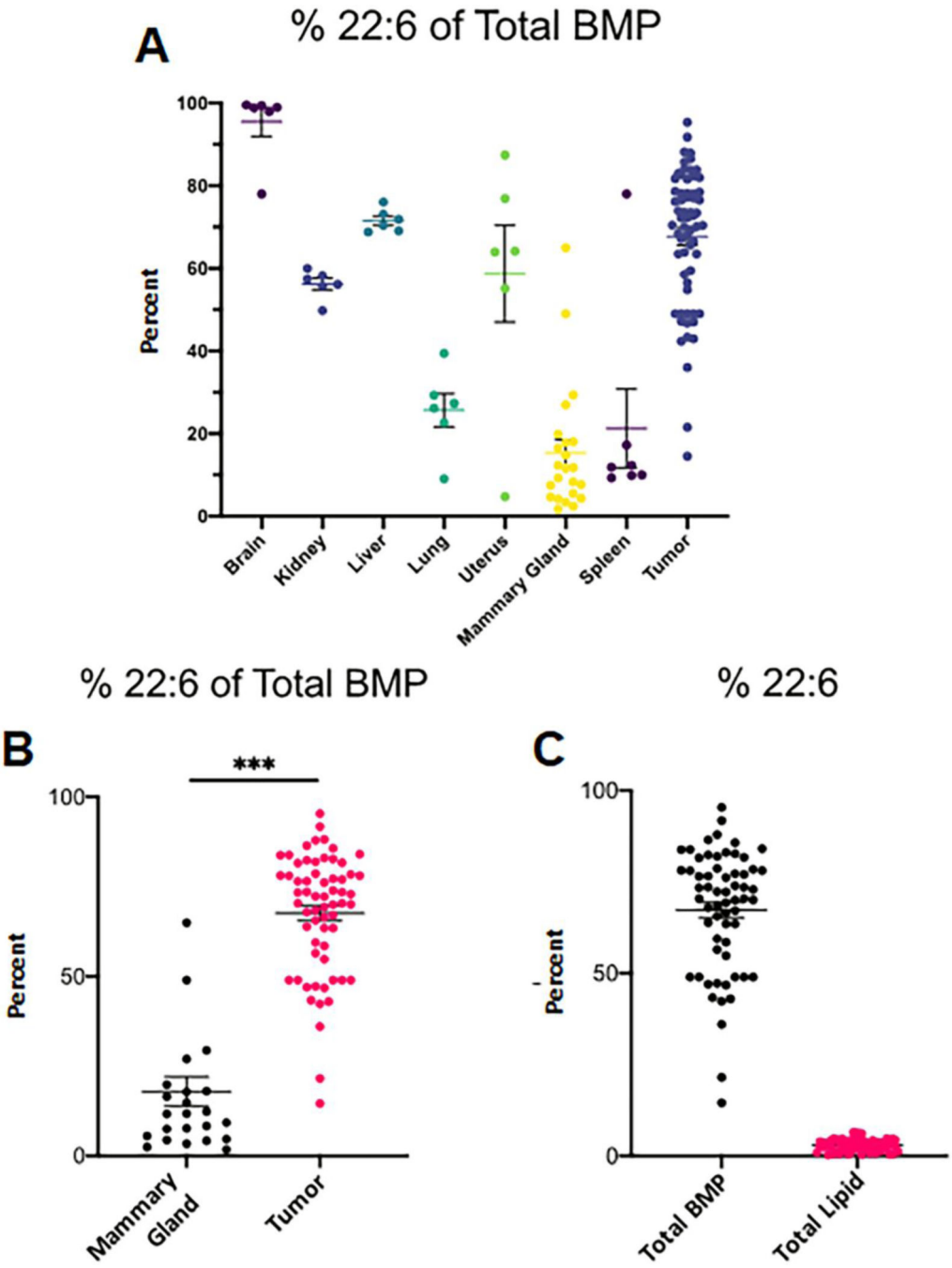

Figure 5. Transformation-associated enrichment of 22:6-containing BMP species is recapitulated in a genetically-engineered mouse model of mammary tumorigenesis.

(A) Purified lipid extract was obtained from MMTV-NDL mouse mammary tumors and matched normal mammary gland, brain, kidney, liver, lung, spleen, and uterus tissues. BMP levels were measured using RPLC-QEHFMS, and the percentage of BMP species consisting of one or more DHA (FA 22:6) side chains relative to total BMP quantity is depicted. **(B)** Enrichment of 22:6-containing BMPs in tumor and normal mammary gland is highlighted. **(C)** The overall fraction of tumor lipids with one or more DHA (FA 22:6) side chain is

Author Manuscript Author Manuscript Author Manuscript Author Manuscript

presented as a percentage of total lipids (BMPs included) and compared with the fraction of 22:6-containing BMPs. Averages for each compound by tissue type are shown, and box plots were drawn using ggplot2 in R statistical program. Normal tissues from $n = 6$ FVB/nJ mice were harvested for these studies, with $n = 24$ distinct mammary glands analyzed ($n = 4$ per mouse). In total, $n = 58$ mammary tumors collected from $n = 12$ MMTV-NDL mice were included in these studies. Significance was determined by ANOVA with Tukey's post-hoc analysis and FDR correction. ***, $P < 0.001$. All P values are presented in Supplementary Table S2.

Author Manuscript Author Manuscript Author Manuscript Author Manuscript

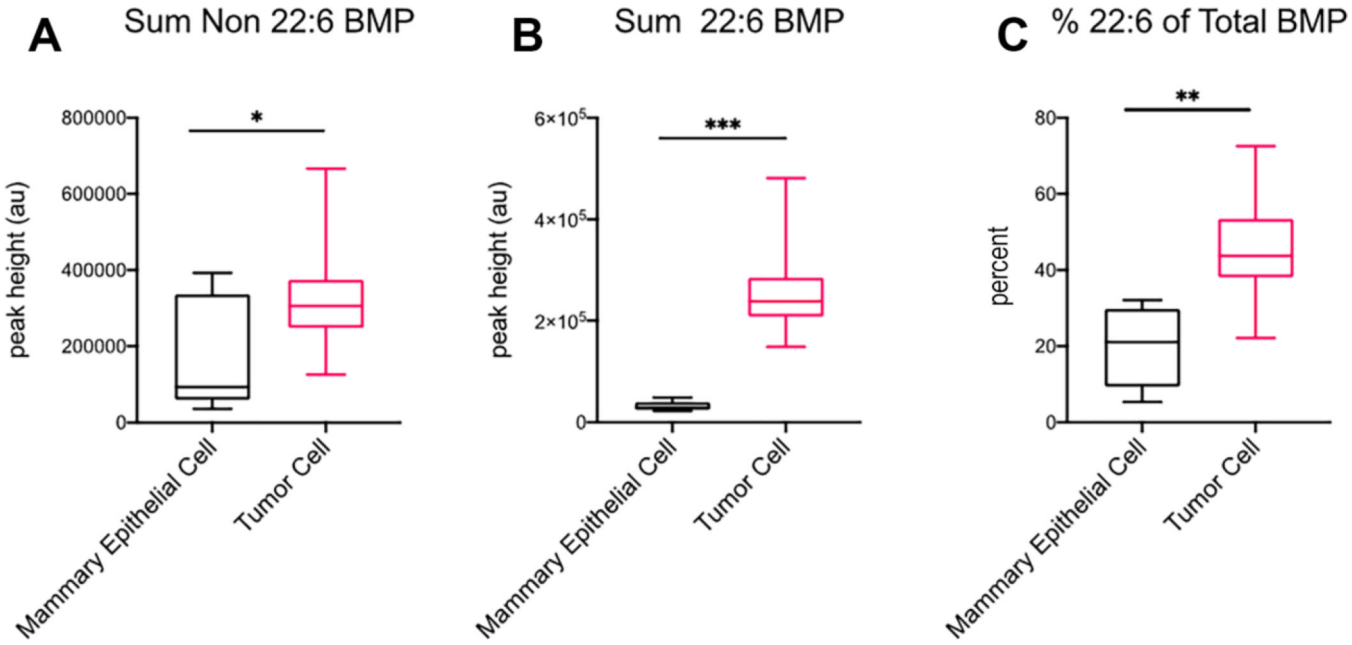

Figure 6. Lipidomics analysis of isolated mouse mammary tumor cells and normal mammary epithelial cells validates cancer-specific 22:6 BMP phenotype.

Tumor cell and mammary epithelial cell populations purified from MMTV-NDL tumors and FVB-nJ mammary glands, respectively, were subjected to RPLC-QEHFMS analysis, and the abundance of summed non-DHA (FA 22:6)-containing **(A)** and 22:6-containing **(B)** BMPs are represented as mass spectrum peak heights. **(C)** The fraction of 22:6 BMPs is displayed as a percentage of total BMP content. Averages for each compound by cell type are shown, and box plots were drawn using ggplot2 in R statistical program. 66 replicate samples of 1×10^6 cells harvested from multiple tumors across $n = 4$ MMTV-NDL mice were analyzed, as were 10 replicate samples of 1×10^6 mammary epithelial cells from $n = 4$ FVB-nJ mice. Significance was determined by *t*-test with Benjamini Hochberg corrected *p*-values. *, $P < 0.05$; **, $P < 0.01$; ***, $P < 0.001$. All *P* values are presented in Supplementary Table S2.

Author Manuscript Author Manuscript Author Manuscript Author Manuscript

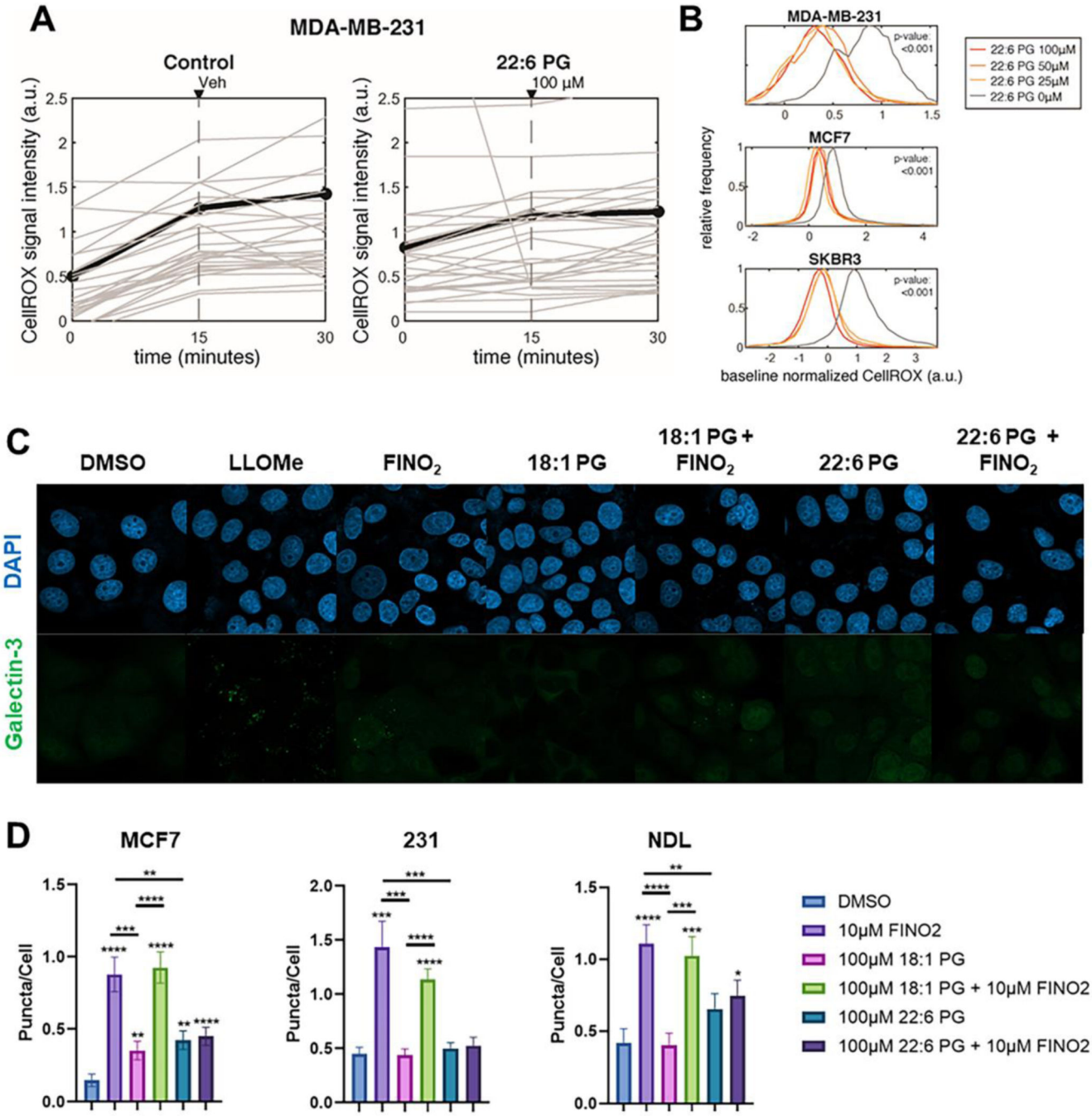

Figure 7. 22:6-containing BMPs scavenge cellular ROS and protect cells from oxidant-induced lysosomal membrane permeabilization.

(A) Time-lapse wide-field microscopy was employed for single cell analysis of CellROX signal, indicating cellular ROS abundance, in response to 22:6–22:6 PG lipid precursor supplementation. MDA-MB-231 single cell (gray) and average (black) signal intensity over a 30-minute time course following 100μM 22:6–22:6 PG supplementation is presented. **(B)** Relative frequency of baseline normalized fluorescent CellROX signal in MDA-MB-231, MCF7, and SKBR3 cancer lines is shown following 30-minute incubation with increasing

Author Manuscript Author Manuscript Author Manuscript Author Manuscript

concentrations of 22:6 PG lipids. Data is representative of three independent time-lapse experiments. Significance was determined by ANOVA with Tukey's post-hoc analysis; $P < 0.001$ for all conditions relative to 0μM lipid. **(C)** MCF7 cells were pre-treated with vehicle, 100μM 18:1 PG or 22:6 PG for 1hr prior to treatment with vehicle or 10μM FINO2 for 8hr, and galectin redistribution into lysosomal puncta was determined by confocal microscopy. LLOMe is a potent LMP inducer and serves as a positive control for galectin relocalization. Representative images from MCF7 cell are shown. **(D)** Puncta per cell for MCF7, MDA-MB-231, and NDL cell lines was calculated and presented as a bar graph. $n = 3$ biological replicates. Significance was determined by student t-test; *, $P < 0.05$, **, $P < 0.01$, ***, $P < 0.001$, ****, $P < 0.0001$.